

Critical behaviour and scaling functions of the three-dimensional $O(6)$ model

S. Holtmann, T. Schulze

Fakultät für Physik, Universität Bielefeld, D-33615 Bielefeld, Germany

Abstract

We numerically investigate the three-dimensional $O(6)$ model on 12^3 to 120^3 lattices within the critical region at zero magnetic field, as well as at finite magnetic field on the critical isotherm and for several fixed couplings in the broken and the symmetric phase. We obtain from the Binder cumulant at vanishing magnetic field the critical coupling $J_c = 1.42865(3)$. The universal value of the Binder cumulant at this point is $g_r(J_c) = -1.94456(10)$. At the critical coupling, the critical exponents $\gamma = 1.604(6)$, $\beta = 0.425(2)$ and $\nu = 0.818(5)$ are determined from a finite-size-scaling analysis. Furthermore, we verify predicted effects induced by massless Goldstone modes in the broken phase. The results are well described by the perturbative form of the model's equation of state. Our $O(6)$ -result is compared to the corresponding Ising, $O(2)$ and $O(4)$ scaling functions. Finally, we study the finite-size-scaling behaviour of the magnetisation on the pseudocritical line.

Keywords: $O(N)$ models; Binder cumulant; Finite-size scaling; Scaling functions

E-mail: holtmann, tschulze@physik.uni-bielefeld.de

1 Introduction

The chiral phase transition of Quantumchromodynamics (QCD) is of great interest for the understanding of the early universe and the physics of heavy ion collisions. For two massless quark flavours it is supposed to be of second order and to lie in the same universality class as the three-dimensional $O(4)$ spin model [1]-[3]. If these assumptions are valid, one can use the knowledge of the spin model to understand the critical behaviour of the QCD phase transition.

It has been shown [4, 5] that the scaling behaviour in lattice simulations with two light quark flavours is indeed comparable to the universal infinite volume scaling function of the $O(4)$ spin model if one uses Wilson fermions, although the Wilson fermion action has no chiral symmetry on the lattice. For staggered fermions however the $O(4)$ scaling function does not match the QCD data. For two flavours on the lattice the staggered fermion action has a remaining $U(1) \times U(1)$ chiral symmetry. As this symmetry lies in the same universality class as the three-dimensional $O(2)$ spin model, the data has also been compared to approximated infinite volume $O(2)$ data. But the $O(2)$ scaling function matches even worse than the $O(4)$ function.

Since the lattice sizes used in QCD are rather small, it might be better to compare the data to universal finite-size-scaling functions. We have indeed found [6] that the finite-size-scaling functions on the pseudocritical line of $O(2)$ and $O(4)$ are compatible with staggered QCD data.

It has turned out problematic to check QCD data for further critical behaviour found in spin models, e.g. the goldstone effect. In QCD with fermions in the fundamental representation the chiral and the deconfinement phase transitions occur at the same temperature. This could change the properties of the chiral phase transition, as additional degrees of freedom are released.

However in QCD with fermions in the adjoint representation (aQCD) the two phase transitions are separated, so one can study them individually. Since the left-handed and right-handed spinors are indistinguishable in the adjoint representation, the chiral symmetry group is $SU(2N_f)$ and not $SU(N_f)_L \times SU(N_f)_R$ as in the fundamental representation. Thus, for two flavours the symmetry group is $SU(4)$, which is isomorph to $SO(6)$, a subgroup of $O(6)$. The universality class of QCD with adjoint fermions therefore has to be that of the $O(6)$ spin model. In this paper our results for the universal properties of this model will be shown, especially the scaling functions, which are needed for our forthcoming study of aQCD, continuing the work of Karsch and Lütgemeier [7].

The model we investigate is the standard $O(6)$ -invariant nonlinear σ -model, which is defined as

$$\beta \mathcal{H} = -J \sum_{\langle x,y \rangle} \vec{\phi}_x \cdot \vec{\phi}_y - \vec{H} \cdot \sum_x \vec{\phi}_x . \quad (1)$$

Here x and y are the nearest-neighbour sites on a three-dimensional hypercubic lattice, $\vec{\phi}_x$ is a 6-component unit vector at site x and \vec{H} is the external magnetic field. The coupling constant J is considered as inverse temperature, therefore $J = 1/T$.

An additional term $\sum_x [\vec{\phi}_x^2 + \lambda(\vec{\phi}_x^2 - 1)^2]$ is often used in the Hamiltonian with λ tuned to minimize leading order corrections to scaling. It is not applied here, because the appropriate λ value of the $O(6)$ model has not been calculated yet, and such a calculation is beyond the scope of this paper.

If $H = |\vec{H}|$ is non-zero we can decompose the spin vector $\vec{\phi}_x$ into a longitudinal (parallel to the magnetic field \vec{H}) and a transverse component

$$\vec{\phi}_x = \phi_x^\parallel \vec{e}_H + \vec{\phi}_x^\perp \quad \text{with} \quad \vec{e}_H = \vec{H}/H . \quad (2)$$

The order parameter of the system, the magnetisation M , is the expectation value of the lattice average ϕ^\parallel of the longitudinal spin component

$$M = \left\langle \frac{1}{V} \sum_x \phi_x^\parallel \right\rangle = \langle \phi^\parallel \rangle , \quad (3)$$

$V = L^3$ is the volume of the lattice with L points per direction.

At zero magnetic field ($H = 0$) there is no special direction and the lattice average of the spins

$$\vec{\phi} = \frac{1}{V} \sum_x \vec{\phi}_x \quad (4)$$

will have a vanishing expectation value on all finite lattices, $\langle \vec{\phi} \rangle = 0$. As an approximate order parameter for M at $H = 0$ one can take [8]

$$M \simeq \langle |\vec{\phi}| \rangle . \quad (5)$$

Nevertheless, we can use $\vec{\phi}$ to define the susceptibilities and the Binder cumulant by

$$\chi_v = V \langle \vec{\phi}^2 \rangle , \quad (6)$$

$$\chi = V (\langle \vec{\phi}^2 \rangle - M^2) , \quad (7)$$

$$g_r = \frac{\langle (\vec{\phi}^2)^2 \rangle}{\langle \vec{\phi}^2 \rangle^2} - 3 . \quad (8)$$

In the following section we describe our simulations at zero magnetic field and estimate the critical coupling J_c from the Binder cumulant, the magnetisation and the susceptibilities. In Section 2 the critical exponents ν , β and γ are determined. With simulations at $H > 0$ in Section 3 we investigate the behaviour of the model on the critical line, in the broken phase and in the symmetric phase. Finally, the resulting data is used in Section 4 to generate the infinite volume scaling function of the magnetisation. Using this data the infinite volume scaling function of the susceptibility and the position of the pseudocritical line are derived in Section 5. A summary and our conclusions are given in Section 6.

L	J -range	N_J	$N_{meas}[1000]$	τ_{int}
12	1.42830 - 1.42900	25	100 - 200	$\lesssim 3$
16	1.42840 - 1.42880	18	100 - 200	$\lesssim 4$
20	1.42840 - 1.42885	19	100 - 200	$\lesssim 6$
24	1.42835 - 1.42885	19	100 - 200	$\lesssim 6$
30	1.42840 - 1.42885	18	100 - 200	$\lesssim 6$
36	1.42840 - 1.42880	17	100	$\lesssim 5$
48	1.42840 - 1.42880	17	100	$\lesssim 6$
60	1.42840 - 1.42880	16	80	$\lesssim 8$
72	1.42840 - 1.42880	16	80	$\lesssim 9$

Table 1: Survey of the Monte Carlo simulations at $H = 0$ for different lattices. Here N_J is the number of different couplings performed in the appropriate J -range; τ_{int} is the integrated autocorrelation time for the energy and N_{meas} the number of measurements per coupling in units of 1000.

2 Simulations at $H = 0$

All our simulations were done on three-dimensional cubic lattices with periodic boundary conditions. We used Wolff's single cluster algorithm as we did in our previous papers (Refs. [6] and [9]-[11]). The $H = 0$ data were taken from lattices with linear extensions $L = 12, 16, 20, 24, 30, 36, 48, 60$ and 72 . Between the measurements we performed 300-600 cluster updates to reduce the integrated autocorrelation time τ_{int} for the energy.

Butera and Comi [12] determined the critical point of the $O(6)$ spin model using a high temperature (HT) expansion as $J_c = 1.42895(6)$. Therefore we generally scanned the range from $J = 1.3$ up to $J = 1.55$ on smaller lattices with careful regard to the critical region close to the J_c -value found in [12] for all lattices. This data was then further analysed using the reweighting method. More details of the simulations near the critical point are presented in Table 1.

2.1 The Critical Point T_c

Obviously any determination of critical values as well as the definition of the reduced temperature

$$t = \frac{T - T_c}{T_c} \quad (9)$$

relies on the exact location of the critical point. Since there is no result from numerical studies, we check the aforementioned value of Butera and Comi first.

We determine T_c by studying the Binder cumulant g_r , which is a finite-size-scaling function

$$g_r = Q_g(tL^{1/\nu}, L^{-\omega}) . \quad (10)$$

The function Q_g depends on the thermal scaling field and on possible irrelevant scaling fields. In this case only the leading irrelevant scaling field proportional to $L^{-\omega}$ is specified, with an unknown $\omega > 0$. Therefore, at the critical point ($t = 0$) g_r ought to be independent of L apart from corrections due to these irrelevant scaling fields. Fig. 1 shows our results for g_r . On the scale of Fig. 1 we observe no deviation from the scaling hypothesis. After a blow-up of the close vicinity of the critical point, as shown in Fig. 2, one sees that the intersection points J_{ip} between the curves of different lattices are not coinciding perfectly at one J . These minor corrections to scaling have to be considered. By expanding the scaling function Q_g to lowest order in both variables one gets for the intersection point J_{ip} of two lattices with sizes L and $L' = bL$

$$J_{ip}(L, b) = J_c + c_1 s(L, b) \quad \text{with} \quad (11)$$

$$s(L, b) = \frac{1 - b^{-\omega}}{b^{1/\nu} - 1} L^{-\omega - 1/\nu} . \quad (12)$$

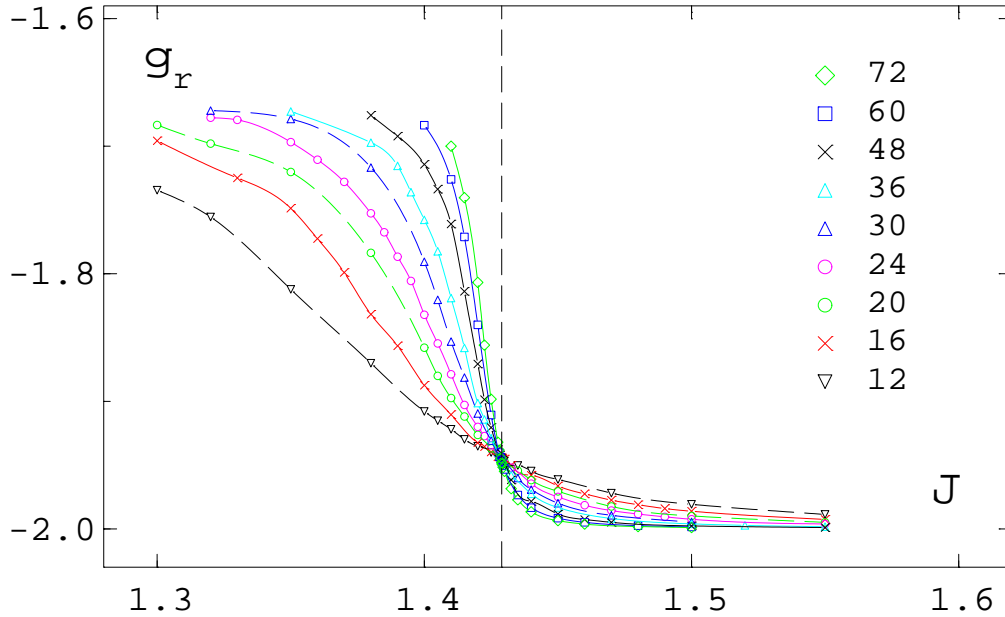


Figure 1: The Binder cumulant g_r from Eq. (8) as a function of the coupling J . The points are connected by splines to guide the eye. With increasing lattice size $L = 12, 16, 20, 24, 30, 36, 48, 60$ and 72 , the slope of the respective curve in the critical region increases. The vertical dashed line denotes our final result for J_c .

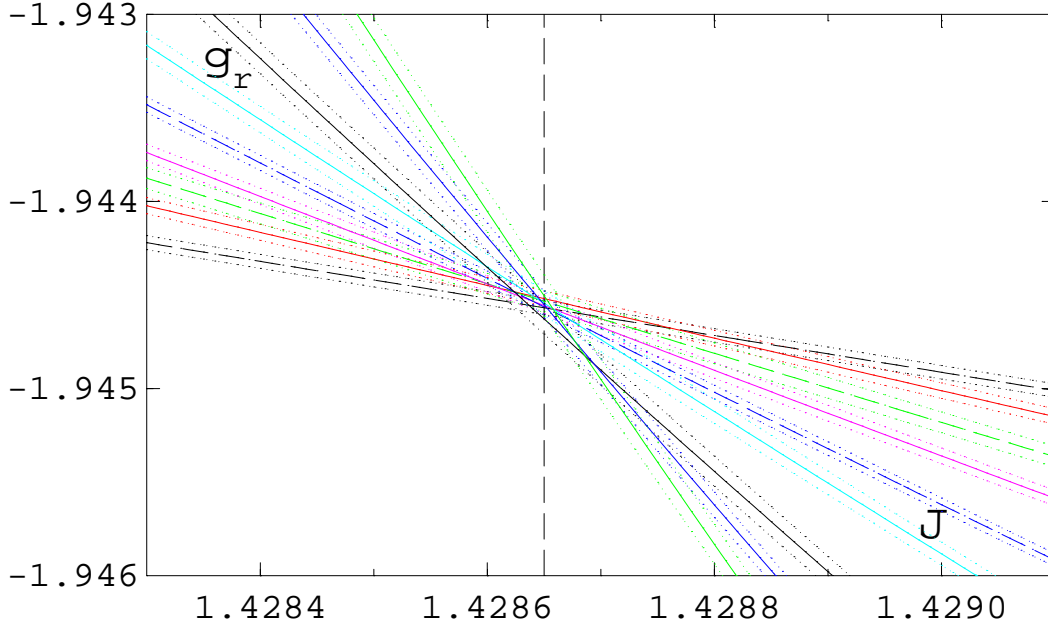


Figure 2: The Binder cumulant g_r in the close neighbourhood of the critical point. The figure is an enlargement of Fig. 1. The dotted lines accompanying the solid/dashed lines show the jackknife error corridors.

To have an unbiased estimate of J_c we choose Binder's approximation [13]

$$\frac{1}{J_{ip}} = \frac{1}{J_c} + \frac{c_2}{\log b}, \quad (13)$$

which can be used without knowing the values of ν and ω . In Fig. 3 the $1/J_{ip}$ values of the intersection points from the lattices $L = 12, 16, 20, 24, 30, 36$ with all other larger lattices are plotted as a function of the variable $1/\log b$ of Eq. (13). Linear fits should lead to the same value $1/J_c$ within the errors. Fitting the results to a constant value and varying the used L -values we find

$$\frac{1}{J_c} = 0.699960(14), \quad (14)$$

which is equivalent to

$$J_c = 1.42865(3). \quad (15)$$

This result agrees in the first four digits with the result $J_c = 1.42895(6)$ of Butera and Comi [12]. There is a slight difference in the last two digits. As this difference is larger than the corresponding errors, we check our result with the χ^2 -method [14] described in the following.

Let us review the general form of the scaling relations for different observables \mathcal{O}

$$\mathcal{O} = L^{\rho/\nu} Q_{\mathcal{O}}(tL^{1/\nu}, L^{-\omega}), \quad (16)$$

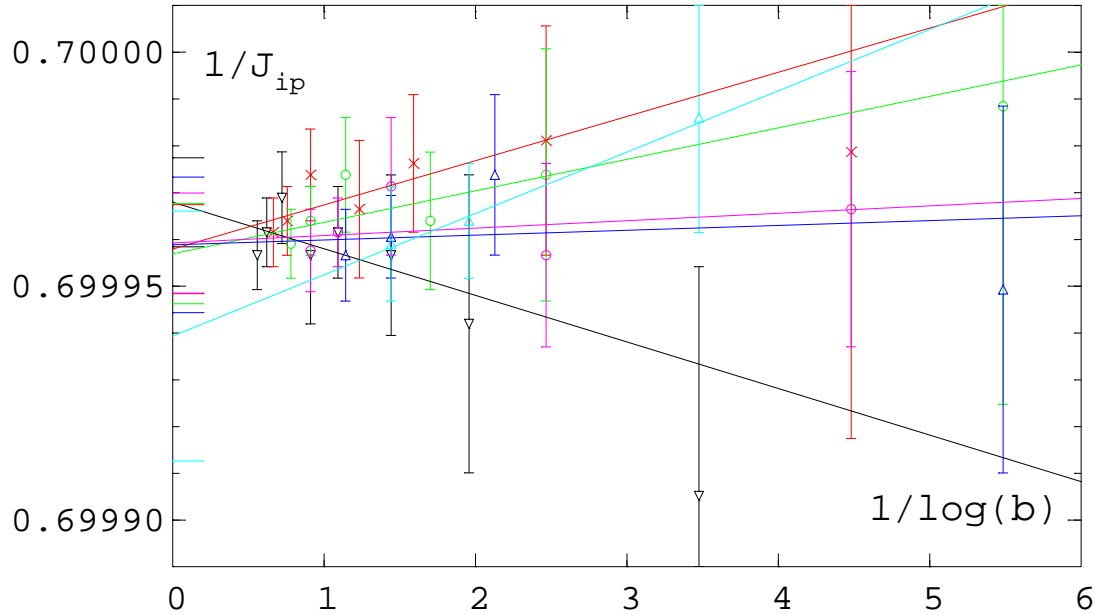


Figure 3: The coupling J_{ip} at the intersection point of $g_r(L)$ and $g_r(bL)$ for various L and b as a function of $1/\log b$, Eq. (13). The solid lines are linear fits for the lattices $L = 12, 16, 20, 24, 30$ and 36 through the intersection points with all larger lattices. The errors of the endpoints are drawn on the ordinate.

where we only take the largest irrelevant exponent into account. Here \mathcal{O} is M , χ or g_r with $\rho = -\beta, \gamma$ and 0 respectively. Expanding the function $Q_{\mathcal{O}}$ to first order in the variables we find

$$\mathcal{O} = L^{\rho/\nu} (c_0 + (c_1 + c_2 L^{-\omega}) t L^{1/\nu} + c_3 L^{-\omega}), \quad (17)$$

which reduces to

$$\mathcal{O} = L^{\rho/\nu} (c_0 + c_3 L^{-\omega}) \quad (18)$$

at the critical point $t = 0$. Therefore at the critical coupling a fit with equation (18) has the minimal χ^2 . Since we do not know the influence of $c_3 L^{-\omega}$ we started without this correction term leaving $L = 12$ out. Fig. 4 (a) shows the result. we find a deviation from our preliminary result in case of the magnetisation M and the susceptibility χ_v . The minima from the Binder cumulant and the susceptibility χ however coincide at $J \approx 1.42865$.

We thereafter made fits with the correction term in the range $\omega = 0.5 - 1.5$. The minimal χ^2 and a perfect agreement of J_c for all observables is found at $\omega = 0.5$. This result is plotted in Fig. 4 (b). $\chi^2/d.o.f.$ increases with ω and shifts J_c in case of M and χ_v to smaller couplings, while the position calculated from χ increases and J_c from g_r remains nearly constant. Since the fits get worse we can exclude ω -values larger than 0.8 . The positions of J_c for $0.5 \leq \omega \leq 0.8$ coincide within the error bars

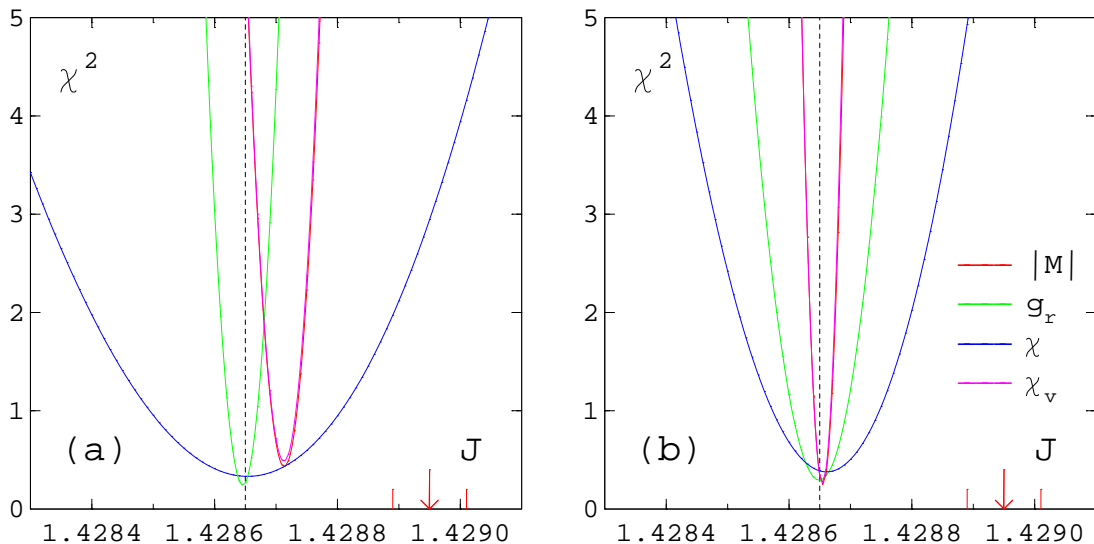


Figure 4: The minimal χ^2 per degree of freedom for fits according to equation (18) for M (red), χ_v (pink), χ (blue) and g_r (green). Figure (a) shows the results without a correcting term $\propto L^{-\omega}$, whereas figure (b) uses $\omega = 0.5$. The dotted black lines show our previous value of J_c , the arrows the result of [12] with its error bars.

of Eq. (15).

At the critical point the Binder cumulant has the form

$$g_r(L) = g_r(J_c) + c_3 L^{-\omega}, \quad (19)$$

with the universal value $g_r(J_c)$ and a small correction term $c_3 L^{-\omega}$. For fits with different ω we find g_r

$$g_r(J_c) = -1.94456(10). \quad (20)$$

The quality of the fits does not change much ($\chi^2/d.o.f. \approx 0.2 - 0.3$) with different ω so a better estimate of ω is still not possible.

2.2 The critical exponents

Since we now know the critical coupling we can study the finite-size behaviour of several observables with Eq. (18). These can be extracted from our reweighted data at T_c . The studied scaling relations are

$$M = L^{-\beta/\nu} (a_0 + a_3 L^{-\omega}), \quad (21)$$

$$\chi = L^{\gamma/\nu} (b_0 + b_3 L^{-\omega}) \quad (22)$$

with $\omega \in [0.5; 1.0[$ and the exponents $-\beta/\nu$ and γ/ν as free parameters. Since these two ratios are connected by the hyperscaling relation

$$\frac{\gamma}{\nu} = 3 - \frac{2\beta}{\nu}, \quad (23)$$

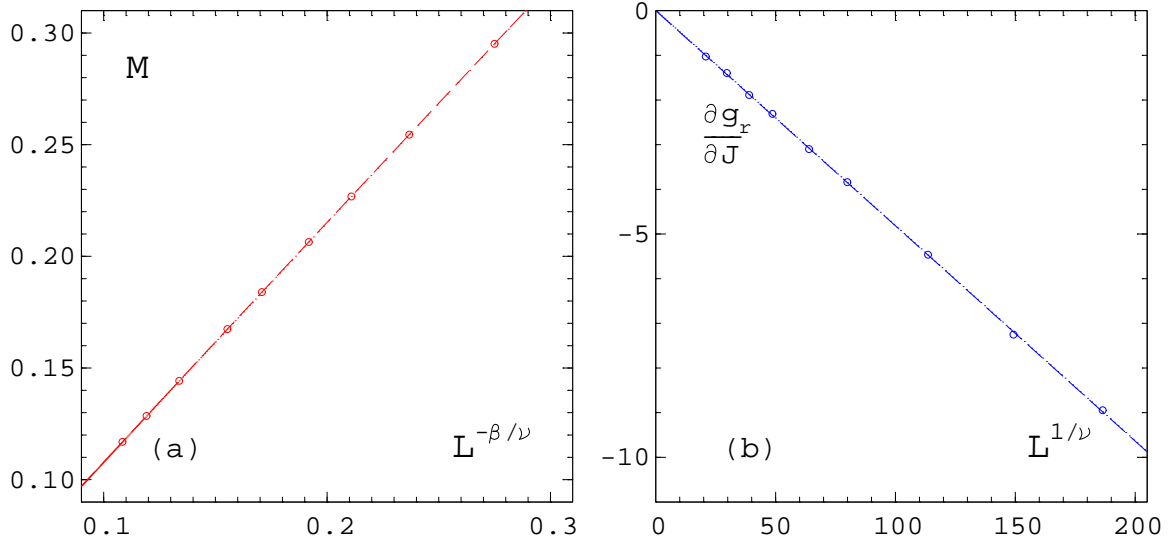


Figure 5: Magnetisation M and the derivative of the binder cumulant $\partial g_r/\partial J$ as a function of the lattice extension L at the critical point T_c and $H = 0$. The dashed line in (a) is a fit to the ansatz (21) for the magnetisation with $\omega = 0.5$. In (b) we used for the derivative of the Binder cumulant the ansatz (24) with $d_3 = 0$ since the corrections are negligible.

Source			exponent	this work	[12]	[15]
$\partial g_r/\partial J$	$1/\nu$	1.223(5)	ν	0.818(5)	0.819(3)	0.790
M	β/ν	0.519(2)	β	0.425(2)	0.424(5)	0.407
χ	γ/ν	1.961(3)	γ	1.604(6)	1.608(4)	1.556

Table 2: The critical exponents for the $O(6)$ model estimated in this work compared to the theoretical work of Butera and Comi [12] and Antonenko and Sokolov [15].

it is necessary to study a further observable, for example the derivative of g_r , which is given at T_c by

$$\frac{\partial g_r}{\partial J} = L^{1/\nu} (d_0 + d_3 L^{-\omega}). \quad (24)$$

In this way two independent exponents (e.g. β and ν) can be estimated. We fit all observables in the range $L = 12 - 72$. From Eq. (21) we obtain

$$\frac{\beta}{\nu} = 0.519(2), \quad (25)$$

in which the error also includes an ω -variation in $[0.5, 1.0]$. Here a larger ω shifts β/ν to a smaller value at nearly constant $\chi^2/d.o.f. \approx 0.4$. Fig. 5 (a) shows the result with $\omega = 0.5$.

Our χ -fits yield

$$\frac{\gamma}{\nu} = 1.961(3). \quad (26)$$

Our results of β/ν and γ/ν are tested with the hyperscaling relation

$$2\frac{\beta}{\nu} + \frac{\gamma}{\nu} = d, \quad (27)$$

with $d = 3$ being the dimension of the model. The left hand side of this equation is 2.999(5), correct within the error.

Finally we analyse the derivative $\partial g_r / \partial J$ of the Binder cumulant at T_c . This observable is directly calculated from the spline connection of our reweighted data in the neighbourhood of the critical point. The errors are obtained with the jackknife method, which seems to underestimate the errors, so we therefore assume the largest error of the different L -values for each lattice. Our fit to ansatz (24) without corrections to scaling ($\chi^2/d.o.f. \approx 0.3$) is shown in Fig. 5 (b). For $d_3 = 0$ we find

$$\frac{1}{\nu} = 1.223(5). \quad (28)$$

The final results of the critical exponents are summarized in Table 2. β and γ are calculated with the result of ν and the ratios (25) and (26). The two last columns of the table show the results from [12] and [15]. Butera and Comi found the same values for the exponents within errors, but the results of Antonenko and Sokolov (given without errors) are farther away.

In the following Sections we use the fixed critical exponents $\beta = 0.425$ and $\nu = 0.818$. The remaining critical exponents are calculated by the respective hyperscaling relations between the critical exponents. For ω we will use the value $\omega = 0.5$, which seems to be the best estimate in all investigations.

3 Simulations at $H > 0$

The magnetisation M is now calculated from equation (3). A transversal and a longitudinal susceptibility can be defined as

$$\chi_L = V(\langle M^2 \rangle - M^2), \quad (29)$$

$$\chi_T = V\langle (\vec{\phi}^\perp)^2 \rangle. \quad (30)$$

We simulated at several constant J -values and increasing magnetic field, starting at $H = 0.00025$. The used lattice sizes were $L = 24, 36, 48, 72, 96$ and 120. Around 20,000 measurements were performed in the (J, H) -regions we used for our fits. The only exception was the data of $L = 120$, where we performed 10,000 measurements at J_c and 5,000 measurements at all other J -values. The integrated autocorrelation

time for the energy and the magnetisation is strongly dependent on the used J -values. At J_c and $J > J_c$ we increased the number of cluster updates between two measurements to have autocorrelation times $\tau_{int} \lesssim 6$.

In the symmetric phase ($J < J_c$) the situation is different. While the measurements of the magnetisation are less correlated with $\tau_{int}(M) \lesssim 4$, the correlation of the energy increases rapidly with decreasing H and J . It reaches values of $\tau_{int}(E) \lesssim 30$ for the larger lattices.

3.1 The critical isotherm

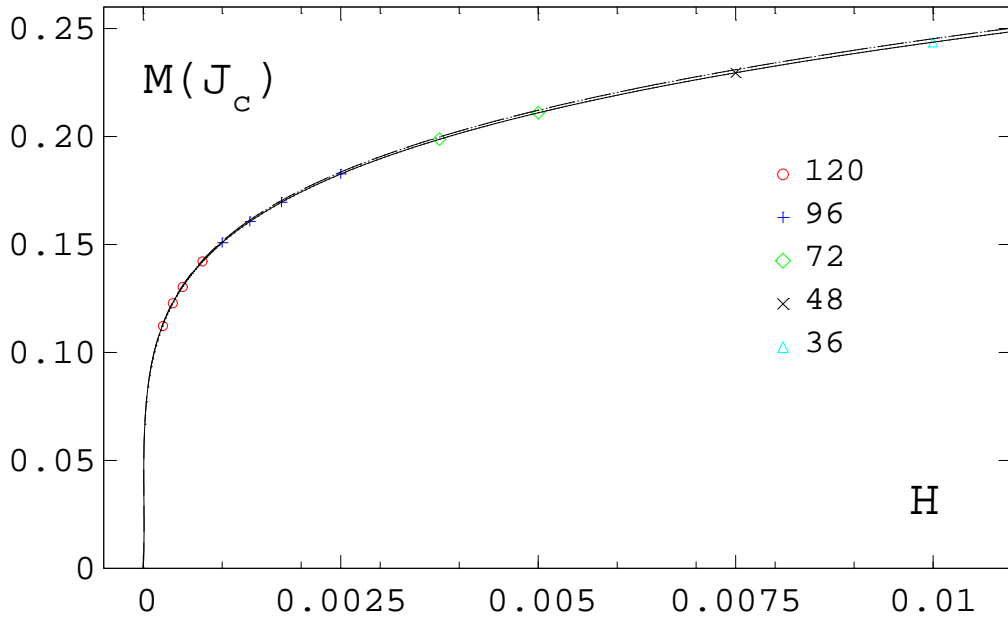


Figure 6: The magnetisation at the critical coupling as a function of H . The solid line is the fit to the ansatz (31), while the dashed line is the leading term.

At the critical point the critical scaling of the magnetisation is given by

$$M(T_c, H) = d_c H^{1/\delta} (1 + d_c^1 H^{\omega_{\nu_c}}), \quad (31)$$

where non-analytic corrections from the leading irrelevant scaling field are taken into account. They are not negligible in our model. The critical exponents δ and ν_c are known from the hyperscaling relations and only depend on the ratio $\beta/\nu = 0.519(2)$:

$$\delta = 3\frac{\nu}{\beta} - 1 = 4.780(22) \quad \text{and} \quad \nu_c = \frac{\nu}{\beta\delta} = 0.4031(24). \quad (32)$$

In order to exclude finite-size effects we carry out a reweighting analysis for all

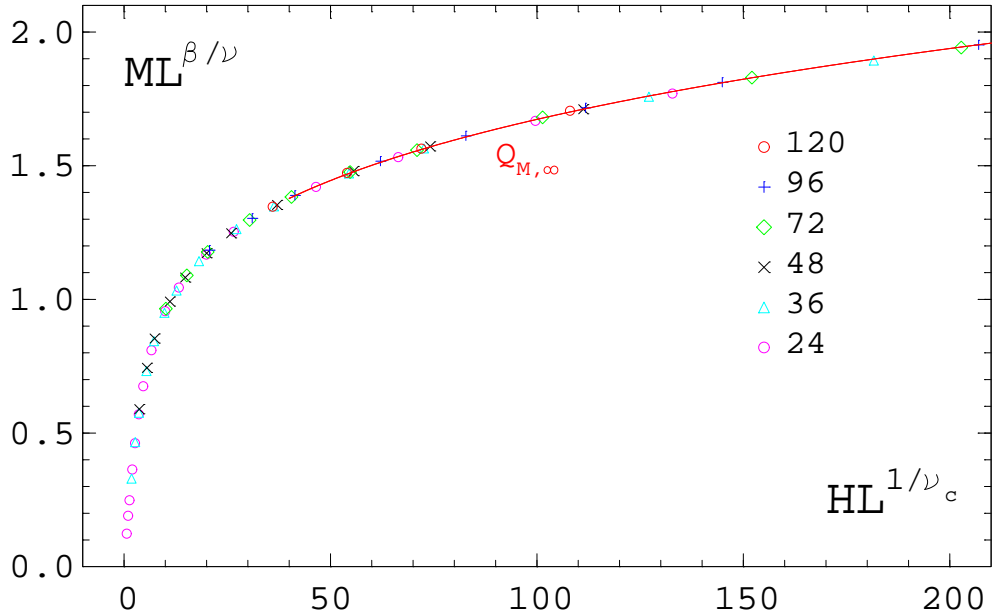


Figure 7: The finite-size-scaling function $Q_{M,\infty}$ on the critical line, Eq. (36). The solid red line indicates the asymptotic function $Q_{0,\infty}$ for $z' \gtrsim 40$.

lattices and fit the result from the largest lattice to approximate the value of $V \rightarrow \infty$. This is done for the interval $H \in [0.00075; 0.04]$ and we find

$$d_c = 0.642(1). \quad (33)$$

Our result is plotted in Fig. 6. There are minimal negative corrections. If one treats δ as a free parameter the result $\delta = 4.79(1)$ agrees with our first estimate.

The finite-size-scaling function for the magnetisation is

$$M(T, H, L) = L^{-\beta/\nu} \Phi(tL^{1/\nu}, HL^{1/\nu_c}, L^{-\omega}). \quad (34)$$

The scaling function Φ can be expanded in $L^{-\omega}$ to

$$M(T, H, L) = L^{-\beta/\nu} \Phi_0(tL^{1/\nu}, HL^{1/\nu_c}) + \dots \quad (35)$$

At T_c the leading part is now given by

$$M(T_c, H, L) = L^{-\beta/\nu} Q_M(z') \quad (36)$$

with the universal scaling function $Q_M(z')$ and the argument $z' = HL^{1/\nu_c}$. The results of all lattices are shown in Fig. 7. The data points scale very well and the influence of corrections to scaling is small. In the limit $z' \rightarrow \infty$ we expect the asymptotic behaviour

$$Q_{M,\infty}(z') = d_c z'^{1/\delta}, \quad (37)$$

which is observable for $z' \gtrsim 40$. This way one checks the value of d_c with a fit of reweighted z' -data of the larger lattices $L = 72, 96, 120$. We find $d_c = 0.642(1)$, which agrees perfectly with our first value of d_c .

3.2 Numerical results at $T \neq T_c$

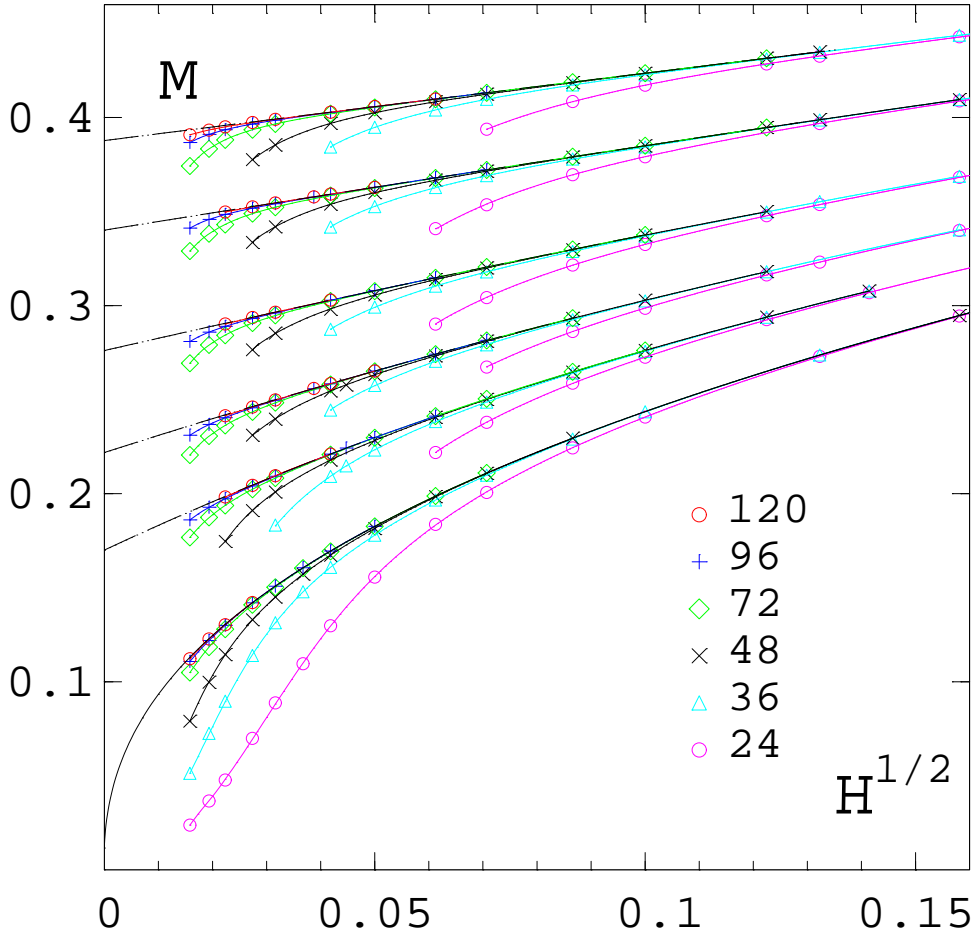


Figure 8: The magnetisation in the broken phase as a function of \sqrt{H} for the couplings $J = 1.6, 1.55, 1.50, 1.47, 1.45$ and J_c and different lattices, starting with the largest J -value at the top. The solid lines represent interpolations from a reweighting analysis of the data. The dashed lines are the fits to ansatz (40) while the solid line is the fit of equation (31) at J_c .

Let us review some perturbative predictions for the magnetisation and the susceptibilities. The continuous $O(6)$ symmetry of our spin model gives rise to spin waves, which are slowly varying (long-wavelength) spin configurations with energies arbitrarily close to the ground-state energy. In $d > 2$ they are massless Goldstone modes associated with the spontaneous breaking of the rotational symmetry for temperatures below the critical value T_c [16]. For $T < T_c$ the system is in a broken phase, i.e. the magnetisation $M(T, H)$ attains a finite value $M(T, 0)$ at $H = 0$.

The transverse susceptibility has the form

$$\chi_T = \frac{M(T, H)}{H} \quad (38)$$

for all H and T . This relation is a direct consequence of the $O(6)$ invariance of the zero-field free energy and can be derived as a Ward identity [17].

The longitudinal susceptibility diverges on the coexistence curve for $2 < d \leq 4$ [18, 19]. The leading terms in the perturbative expansion for three dimensions are

$$\chi_L(T < T_c, H) = b_0(T) H^{-1/2} + c_2(T) . \quad (39)$$

Since the susceptibility is the derivative of the magnetisation with respect to H we find for the magnetisation

$$M(T < T_c, H) = M(T, 0) + c_1(T) H^{1/2} + c_2(T) H \quad (40)$$

near the coexistence curve. Fig. 8 shows our results of the magnetisation in the broken phase and the corresponding extrapolations to $M(T, 0)$ in the thermodynamic limit ($V \rightarrow \infty$). The numbers of the parameters are presented in Table 3. The H -extension of the regions, where the predicted Goldstone behaviour is found, increases with J , while finite-size effects become larger at small H and larger J ($L \gtrsim 160$ would be necessary for finite-size independent data).

$J = 1/T$	$M(T, 0)$	$c_1(T)$	$c_2(T)$	$10^4 \cdot H$	χ^2/dof
1.45	0.1701(03)	1.339(15)	-2.86(18)	9-25	0.45
1.47	0.2219(02)	0.924(02)	-1.138(14)	12-74	0.56
1.50	0.2761(01)	0.659(01)	-0.436(08)	10-93	0.27
1.55	0.3401(01)	0.463(01)	-0.141(02)	10-163	0.78
1.60	0.3878(01)	0.363(01)	-0.047(01)	19-175	0.49

Table 3: Parameters of the fit of $M(T < T_c, 0)$ to the ansatz (40). The fifth column is the used fit range.

We fitted the values of $M(T, 0)$ to the form

$$M(T \lesssim T_c, 0) = B (T_c - T)^\beta [1 + b_1 (T_c - T)^{\omega\nu} + b_2 (T_c - T)] \quad (41)$$

with fixed values $\beta = 0.425$, $\omega\nu = 0.409$ and the result

$$B = 1.22(1), \quad (42)$$

$b_1 = -0.184(49)$ and $b_2 = 0.31(13)$. The error of B also includes the slight uncertainty in the value of $\omega\nu$. Our final result of $M(T, 0)$ and the difference to the leading term are plotted in Fig. 9(a).

Since one of the main aims of this work is the determination of the magnetic equation of state in Section 4, we also simulated in the high temperature phase. Again we use data of the largest lattices as an approximation for the infinite volume value. The result is plotted in Fig. 9(b). From a Taylor expansion we expect

$$M(T > T_c, H) \propto H. \quad (43)$$

at small H . With increasing temperature the H -interval with this behaviour increases, as one can see in Fig. 9(b).

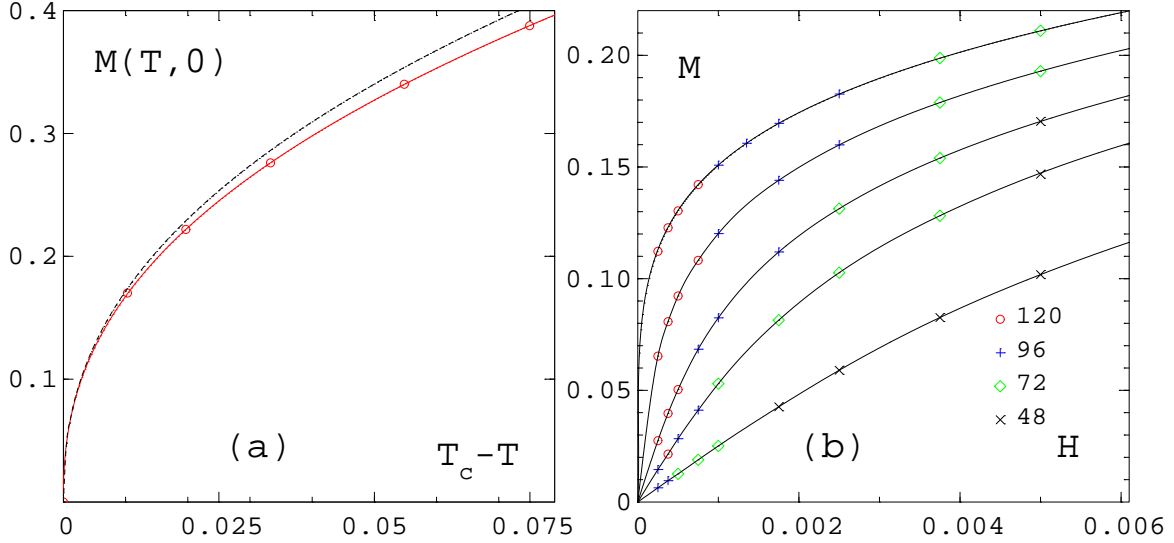


Figure 9: (a) Magnetisation $M(T,0)$ on the coexistence curve as a function of $(T_c - T)$. The red line is the fit to ansatz (41) while the black dashed line is the leading part. (b) shows the magnetisation in the symmetric phase ($T \geq T_c$) as a function of H , starting from the top with fixed $J = J_c, 1.42, 1.41, 1.40$ and 1.38 and different L -values. The lines are spline connections between the data points.

4 The Scaling function

The critical behaviour of the magnetisation in the vicinity of T_c is described by the general Widom-Griffiths form [20]

$$y = f(x) \quad (44)$$

with

$$y \equiv h/M^\delta, \quad x \equiv t'/M^{1/\beta}, \quad (45)$$

where the variable t' is proportional to $(T - T_c)$ and h proportional to H . A common normalisation of the function $f(x)$ is

$$f(0) = 1, \quad f(-1) = 0. \quad (46)$$

The variables t' and h are the conveniently normalized reduced temperature $t' = (T - T_c)/T_0$ with $T_0 = B^{-1/\beta} = 0.626(12)$ and the reduced magnetic field $h = H/H_0$ using $H_0 = d_c^{-\delta} = 8.32(6)$. The function $f(x)$ is universal and was derived from the ϵ -expansion ($\epsilon = 4 - d$) to order ϵ^2 [17]. In the limit $x \rightarrow -1$, i.e. at $T < T_c$ and close to $H = 0$ the result was inverted to give $x + 1$ as a double expansion in powers of y and $y^{d/2-1}$ [19]

$$x + 1 = \tilde{c}_1 y + \tilde{c}_2 y^{d/2-1} + \tilde{d}_1 y^2 + \tilde{d}_2 y^{d/2} + \tilde{d}_3 y^{d-2} + \dots \quad (47)$$

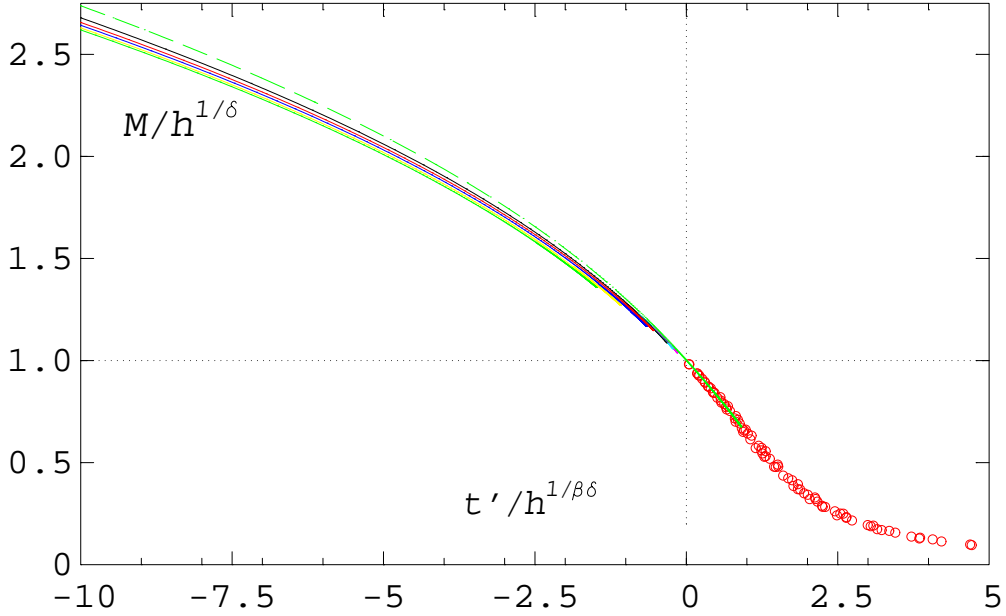


Figure 10: The function $M/h^{1/\delta}$ (dashed green line). The solid lines in the broken phase are the reweighted results for $M/h^{1/\delta}$ at $J = 1.60, 1.55, 1.50, 1.47, 1.45, 1.445$ and 1.44 , from the bottom to the top. The results for 1.445 and 1.44 are very close to $z = 0$. The circles are single data points in the symmetric phase.

The coefficients \tilde{c}_1 , \tilde{c}_2 and \tilde{d}_3 are thereafter obtained from the general expression of [17].

In the large- x limit (corresponding to $T > T_c$ and small H), the expected behaviour is given by Griffiths's analyticity condition [20]

$$f(x) = \sum_{n=1}^{\infty} a_n x^{\gamma-2(n-1)\beta}. \quad (48)$$

The form (44) of the equation of state is equivalent to the often used relation

$$M = h^{1/\delta} f_G(z), \quad (49)$$

where f_G is a further universal scaling function and z the combination

$$z = t'/h^{1/\beta\delta}. \quad (50)$$

The normalisation conditions of $f_G(z)$ are

$$f_G(0) = 1 \quad \text{and} \quad f_G(z) \xrightarrow{z \rightarrow -\infty} (-z)^\beta. \quad (51)$$

This version is normally used for comparison to QCD lattice data. The function $f(x)$ is connected with $f_G(z)$ by

$$y = f_G^{-\delta}, \quad x = z f_G^{-1/\beta}. \quad (52)$$

These scaling functions are only valid close to J_c and $H \rightarrow 0$. First tests show that the data we have used in the broken phase does not scale directly, while in the high temperature phase most of the data scales close to T_c and small H . So we used a more general form of (49)

$$Mh^{-1/\delta} = \Psi(z, h^{\omega\nu_c}) \quad (53)$$

with a scaling function Ψ , which can be expanded to

$$Mh^{-1/\delta} = f_G(z) + h^{\omega\nu_c} f_G^{(1)}(z) + h^{2\omega\nu_c} f_G^{(2)}(z) + \dots \quad (54)$$

This way in the broken phase one obtains the leading part f_G by quadratic fits to our data in $h^{\omega\nu_c}$ at constant z -values and different (J/H) -combinations. But we are only able to correct the data with $z \lesssim -2$ because we have not enough J -values closer to J_c to make the fits. In Fig. 10 we show the influence of the corrections and the final scaling function f_G in the broken phase (dashed green line).

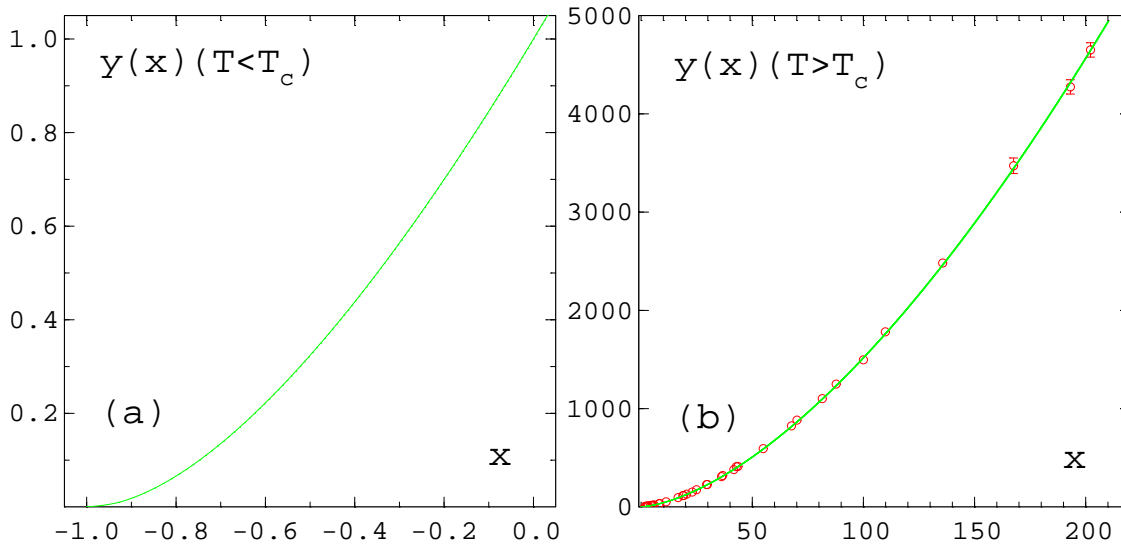


Figure 11: The functions $y = f(x)$ at small x (a) and large x -values (b). In figure (a) we plot the fit to ansatz (55) using extrapolated data in the broken phase and data-points in the symmetric phase. In (b) we plot data-points of the symmetric phase and the fit to ansatz (48) using the first three terms.

Our result for $f_G(z)$ can be transformed with (52) into the Widom-Griffiths form of the equation of the state (44). Unfortunately the z -interval we used to extract $f_G(z)$ is only equivalent to the small region $-0.9 \lesssim x \lesssim -0.7$, which can be used for a fit. We use the three leading terms in (47)

$$x_1(y) + 1 = (\tilde{c}_1 + \tilde{d}_3) y + \tilde{c}_2 y^{1/2} + \tilde{d}_2 y^{3/2}. \quad (55)$$

Since $y(0) = 1$ the coefficients are connected by $\tilde{d}_2 = 1 - (\tilde{c}_1 + \tilde{d}_3 + \tilde{c}_2)$. Fits to x in the interval $-0.9 \lesssim x \lesssim -0.7$ and points in the symmetric phase with $0.2 \lesssim x \lesssim 2.9$,

$1.4 \lesssim J < J_c$ and $H \leq 0.0015$ lead to

$$\tilde{c}_1 + \tilde{d}_3 = 0.36(5), \quad \tilde{c}_2 = 0.69(3). \quad (56)$$

The result of the fit is shown by the green line in Fig. 11(a).

For large x we use a 3-parameter fit of the first three terms of Griffiths's analyticity condition (48)

$$y_2(x) = a_1 x^\gamma + a_2 x^{\gamma-2\beta} + a_3 x^{\gamma-4\beta} \quad (57)$$

in the interval $x \in [1.75, 202]$ and data points restricted to $1.4 \lesssim J < J_c$ and $H \leq 0.0015$. We find

$$a_1 = 0.92(1), \quad a_2 = 1.17(2), \quad a_3 = 0.91(3). \quad (58)$$

This result is plotted in Fig. 11(b). With the coefficient a_1 of the leading part one can calculate the universal ratio

$$R_\chi = a_1^{-\gamma} = 1.14(2). \quad (59)$$

The $O(6)$ scaling function f_G can be parametrically obtained from $x_1(y)$ and $y_2(x)$,

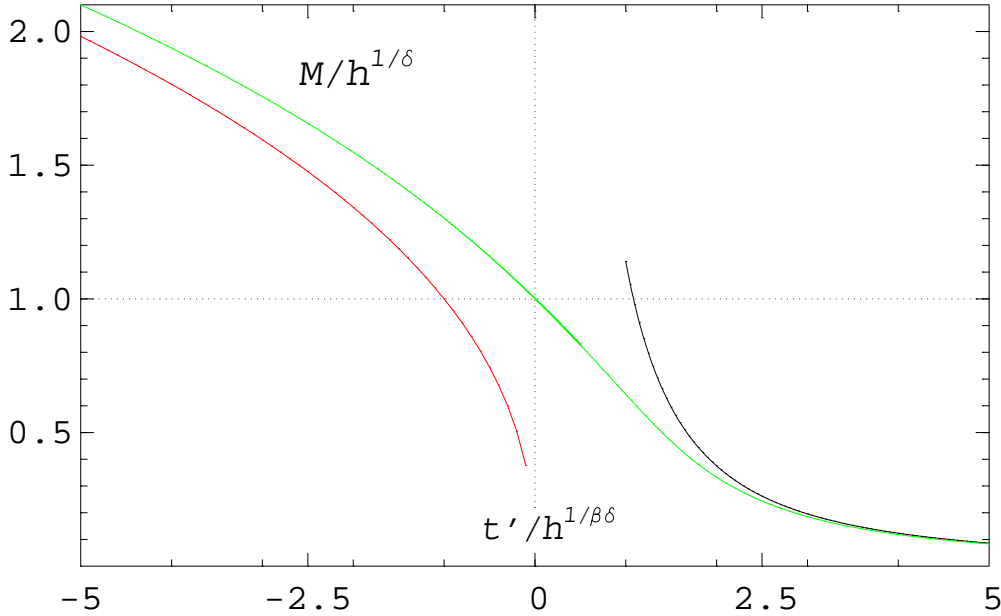


Figure 12: The scaling function f_G of the $O(6)$ model (green) and the asymptotic behaviours for $z \rightarrow \infty$ (black) and $z \rightarrow -\infty$ (red).

which is connected by a spline between $z = 0.5$ and $z = 0.8$, where we have no reliable parametrisation. The result is plotted in Fig. 12. Also plotted are the leading terms of the asymptotic behaviour at $z \rightarrow \pm\infty$. These are

$$f_G(z) \underset{z \rightarrow -\infty}{=} (-z)^\beta, \quad (60)$$

$$f_G(z) \underset{z \rightarrow +\infty}{=} R_\chi z^{-\gamma} \quad (61)$$

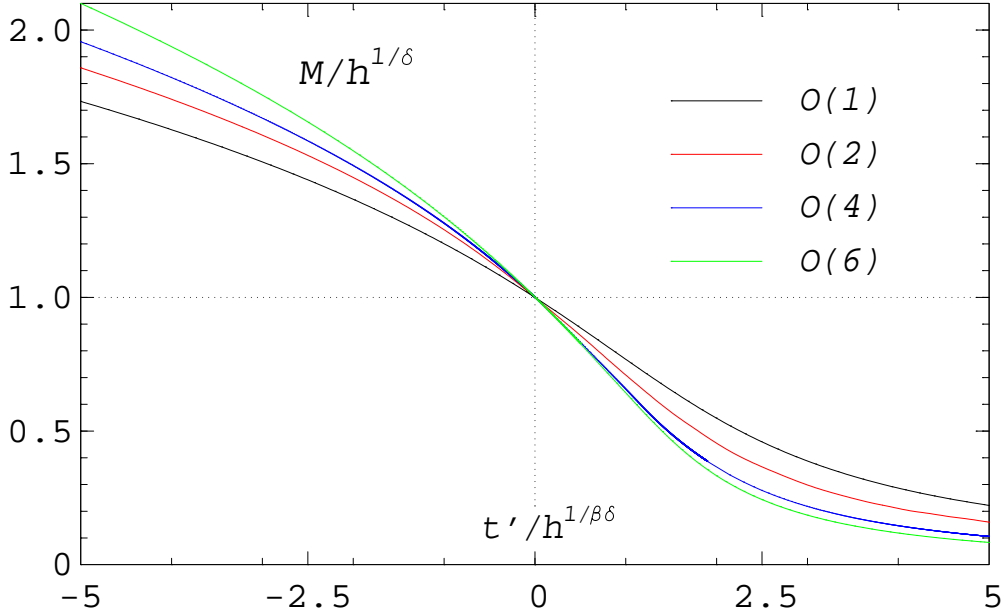


Figure 13: The scaling function f_G for the Ising (black), $O(2)$ (red), $O(4)$ (blue) and $O(6)$ model (green).

according to the normalisation (51). The fact that for large temperatures and small H the magnetisation is proportional to H , see Eq. (43), explains the asymptotic behaviour for $z \rightarrow \infty$. In the symmetric phase the asymptotic behaviour is reached for small absolute values of z , while in the broken phase the scaling function converges to the asymptotic form not until large absolute values of z .

Finally, the $O(6)$ scaling function f_G can be compared to the corresponding functions for the Ising ($O(1)$) model [21], the $O(2)$ [10] and the $O(4)$ model [9], shown in Fig. 13. All functions have a similar shape.

5 The Pseudocritical Line

In order to discuss finite-size-scaling functions in an easier way, it is common to study lines of constant z -values. There one expresses H as a function of T or vice versa. Important examples of lines of fixed z are the critical line ($z = 0$), discussed in Section 3.1, and the pseudocritical line $z = z_p = \text{const}$, the line of peak positions of the susceptibility χ_L in the (t, h) -plane for $V \rightarrow \infty$. There are two different ways to find that value of z_p for $O(N)$ models. One way is to locate the peak positions of χ_L as a function of the temperature at different fixed small values of the magnetic field on lattices with increasing size L^3 . The scaling function, on the other hand, offers a more elegant way to determine the pseudocritical line. Since χ_L is the derivative of

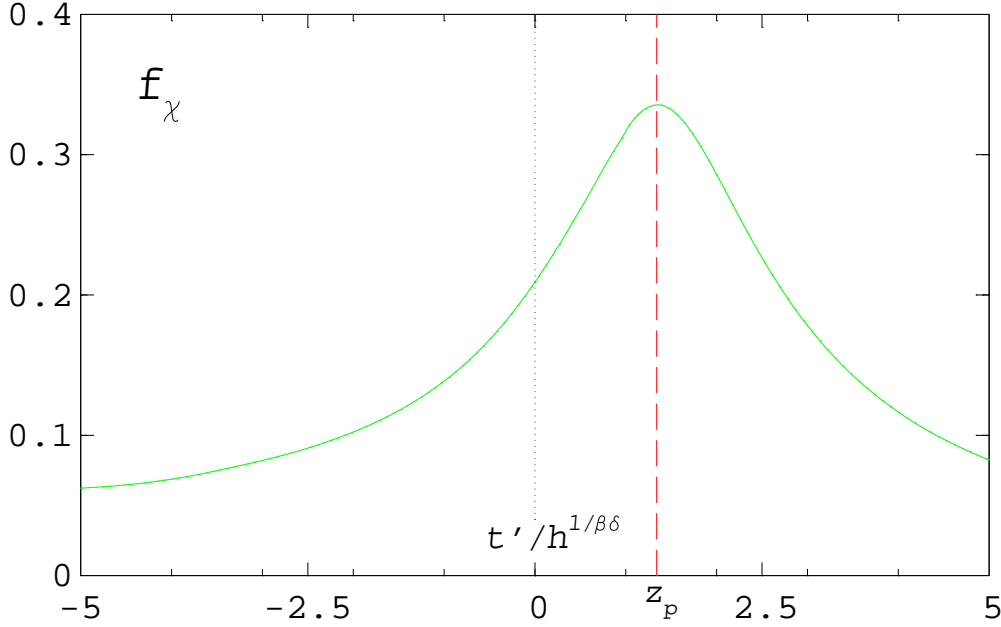


Figure 14: The scaling function f_χ for the $O(6)$ model. The dashed red line shows the position of $z_p = 1.34$.

M

$$\chi_L = \frac{\partial M}{\partial H} = \frac{h^{1/\delta-1}}{H_0} f_\chi(z), \quad (62)$$

its scaling function $f_\chi(z)$ can be calculated directly from $f_G(z)$

$$f_\chi(z) = \frac{1}{\delta} \left(f_G(z) - \frac{z}{\beta} \frac{\partial f_G}{\partial z}(z) \right). \quad (63)$$

The maximum of $f_\chi(z)$ is located at z_p , which is another universal quantity. We find for the $O(6)$ model

$$z_p = 1.34(5). \quad (64)$$

The error includes the fit-errors of the parameters in (58).

In Fig. 14 we show the result for $f_\chi(z)$ from Eq. (63) in the $O(6)$ model.

At z_p a finite-size-scaling analysis in the variables H and L can be performed. Eq. (35) reduces to

$$M(H, L) = L^{-\beta/\nu} Q_{z_p}(hL^{1/\nu_c}) + \dots \quad (65)$$

with another universal scaling function Q_{z_p} . The asymptotic form $Q_{z_p, \infty}$ of Q_{z_p} is

$$Q_{z_p} \rightarrow Q_{z_p, \infty} = f_G(z_p) (hL^{1/\nu_c})^{1/\delta} \quad \text{for } L \rightarrow \infty. \quad (66)$$

The results are presented in Fig. 15(a). The data does not scale directly but with increasing volume the data-points approach Q_{z_p} from the top. In Fig. 15(b) we plotted the data in a double-log form and find that the asymptotic form $Q_{z_p, \infty}$ coincides

with the Q_{z_p} -value of the largest lattice extension at $HL^{1/\nu_c} \gtrsim 42$. Therefore Q_{z_p} is asymptotic. At smaller values, one observes an approach of Q_{z_p} from below to $Q_{z_p, \infty}$.

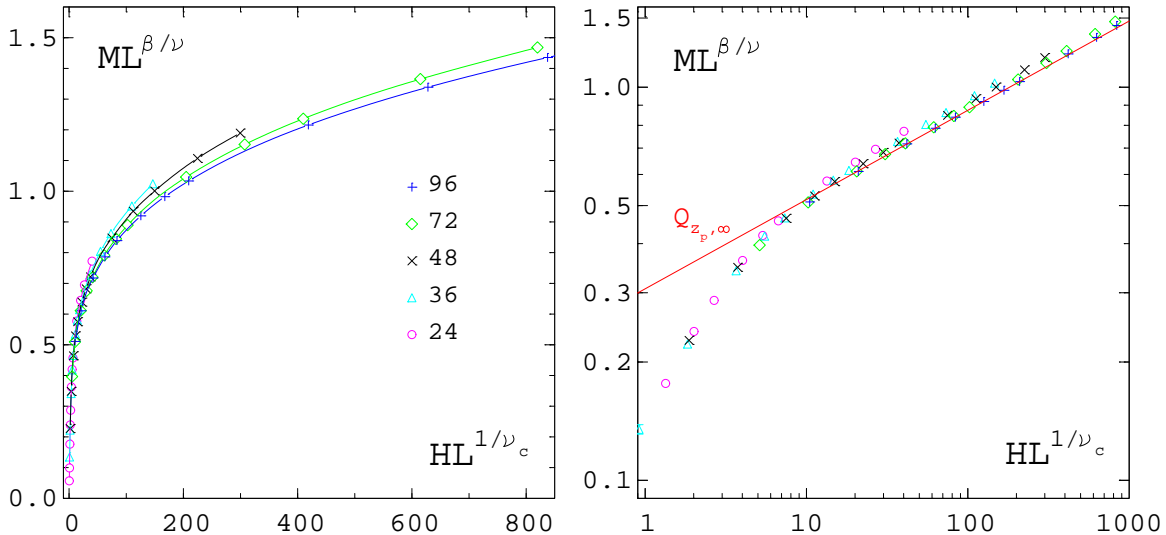


Figure 15: (a) Finite-size scaling of $ML^{\beta/\nu}$ on the pseudocritical line. The solid line shows the asymptotic form $Q_{z_p, \infty}$, the symbols denote different lattice sizes L . (b) is a double-log plot of (a).

6 Conclusions

In this paper we calculated several important quantities of the $O(6)$ spin model directly from Monte Carlo simulations on cubic lattices. At zero external field we determined the critical coupling J_c by a finite-size-scaling analysis of the Binder cumulant and by the χ^2 -method. Our result agrees in the first four digits with the result of Butera and Comi. At the critical point we estimated the critical exponents from finite-size-scaling fits. We obtained β from the magnetisation, γ from the susceptibility and ν from the derivative of the Binder cumulant. Our results are in accord with the values found by Butera and Comi but slightly different compared to the values found by Antonenko and Sokolov. We find small corrections to scaling for all observables.

On the critical line $T = T_c, H > 0$ and in the limit $V \rightarrow \infty$, the critical amplitude d_c of the magnetisation was computed. We found small negative corrections to scaling and checked the finite-size-scaling behaviour of M at T_c and its asymptotic form. Below the critical temperature, we investigated the behaviour of M at several couplings J as a function of $H^{1/2}$ in the limit $V \rightarrow \infty$. Close to the coexistence line, i.e. small $H \rightarrow 0$, the predicted Goldstone behaviour was observed. We were able

to extrapolate our data to the values $M(T < T_c; H = 0)$ of the infinite volume limit, fitted these M -values with the corresponding ansatz, and estimated the critical amplitude B of the magnetisation. In this case the corrections to scaling were again negative and more pronounced as on the critical line. At high temperatures and $H > 0$, we observe the expected proportional dependence on H of the magnetisation.

We used our data of the largest lattices in the low and high-temperature phase to parametrise the scaling function f_G of the $O(6)$ model. We encountered large corrections to scaling in the broken phase, while most data in the symmetric phase scales directly. By generalizing f_G to include corrections to scaling, our group extracted a part of f_G in the broken phase and fitted the result combined with direct data points in the symmetric phase. On the other hand, we fitted data of the symmetric phase using Griffiths's analyticity condition. Finally, we compared our $O(6)$ -result for f_G with the corresponding scaling functions of the $O(1)$, $O(2)$ and $O(4)$ model. These functions are clearly distinguishable and in a systematic order. We use our result of f_G to calculate the scaling function f_χ of the susceptibility. From the position of the maximum in f_χ the location of the pseudocritical line was determined. There we made finite-size-scaling plots and found considerable corrections to scaling. The data of smaller lattices approaches the universal finite-size-scaling function from above. The asymptotic form of the universal part is reached at $HL^{1/\nu_c} \approx 42$. A comparison between the $O(6)$ model and aQCD will be done in the near future.

Acknowledgements

We are grateful to Jürgen Engels and Sandra Wanning for reading this manuscript carefully. Our work was supported by the Deutsche Forschungsgemeinschaft under Grant No. FOR 339/1-2.

References

- [1] R. D. Pisarski and F. Wilczek, Phys. Rev. D **29** (1984) 338.
- [2] K. Rajagopal and F. Wilczek, Nucl. Phys. B **399** (1993) 395.
- [3] F. Wilczek, Int. J. Mod. Phys. A **7** (1992) 3911.
- [4] S. Aoki *et al.* [JLQCD Collaboration], Nucl. Phys. Proc. Suppl. **60A** (1998) 188.
- [5] S. Aoki, Y. Iwasaki, K. Kanaya, S. Kaya, A. Ukawa and T. Yoshie, Nucl. Phys. Proc. Suppl. **63** (1998) 397.
- [6] J. Engels, S. Holtmann, T. Mendes and T. Schulze, Phys. Lett. B **514** (2001) 299.

- [7] F. Karsch and M. Lütgemeier, Nucl. Phys. B **550** (1999) 449.
- [8] A. L. Talapov and H. W. Blöte, J. Phys. A **29** (1996) 5727.
- [9] J. Engels and T. Mendes, Nucl. Phys. B **572** (2000) 289.
- [10] J. Engels, S. Holtmann, T. Mendes and T. Schulze, Phys. Lett. B **492** (2000) 219.
- [11] A. Cucchieri, J. Engels, S. Holtmann, T. Mendes and T. Schulze, J. Phys. A **35** (2002) 6517.
- [12] P. Butera and M. Comi, Phys. Rev. B **58** (1998) 11552.
- [13] K. Binder, Phys. Rev. Lett. **47** (1981) 693.
- [14] J. Engels, S. Mashkevich, T. Scheideler and G. Zinovev, Phys. Lett. B **365** (1996) 219.
- [15] S. A. Antonenko and A. I. Sokolov, Phys. Rev. E **51** (1995) 1894.
- [16] See e.g. V.G. Vaks, A.I. Larkin and S.A. Pikin, Sov. Phys. JETP **26** (1968) 647.
- [17] E. Brézin, D.J. Wallace and K.G. Wilson, Phys. Rev. B **7** (1973) 232.
- [18] J. Zinn-Justin, Clarendon Press, Oxford, 1996; R. Anishetty et al., Int. J. Mod. Phys. A **14** (1999) 3467.
- [19] D. J. Wallace and R. K. P. Zia, Phys. Rev. B **12** (1975) 5340.
- [20] R. B. Griffiths, Phys. Rev. **158** (1967) 176.
- [21] J. Engels, L. Fromme and M. Seniuch, Nucl. Phys. B **655** (2003) 277.